Application of Fibre-Optic Interferometry to Detection of Human Vital Signs

Damjan Zazula, Denis Đonlagić, Sebastijan Šprager
University of Maribor, Faculty of Electrical Engineering and Computer Science, Smetanova ulica 17, SI-2000 Maribor, Slovenia

ABSTRACT

Ageing population and limited healthcare budgets call for new paradigms and more efficient healthcare and medical services. Home and continuous care for the elderly and people with disabilities can facilitate and prolong their independent living. The core solution is unobtrusive observations of human vital functions. Sensors being capable of detecting several vital sign at a time are of particular interest.

This paper introduces a new healthcare monitoring technology based on fibre-optic interferometry which detects sub-micron changes of optical fibre length. Mechanical and acoustic activity of human heart causes changes of a few microns. We model the observed interferometric signal by a superimposition of all external fibre stimuli. These can be extracted by unwrapping the phase of the analytic version of intereferometric signal. We then process the unwrapped phase by modified continuous wavelet transform whose multiresolution properties sort out different signal components.

Our main finding is that Morlet-wavelet-based transform of fibre-optic interferometric signal can separate ballistocardiographic and phonocardiographic components of detected heart activity. To confirm the locations of extracted components are representative, we compute their delays after referential R waves and compare their inter-beat intervals to referential RR intervals. Delays fall within the expected physiological limits, except for the second heart sound which split into two differently delayed groups. This may be explained by well-known fact that aortic and pulmonary valves that generate the second heart sounds may not close synchronously. The inter-beat intervals are best aligned in the first heart sound with P_{90} error below 10%.

Key words: fibre-optic interferometry, human vital signs detection, continuous wavelet transform, ballistocardiography, phonocardiography

I. INTRODUCTION

Rapid development of body sensors contributes to a number of innovations in the areas of telemetry, home care, continuous care, care for elderly and people with disabilities, facilitation of independent living, etc. Several sensors and systems have evolved to the point of being ready for clinical application. Trends show a considerable growth in the use of this technology and suggest that soon wearable sensors and systems will become a part of routine clinical examinations. They are mainly used for simultaneously monitoring of different human vital signs, such as heart rate, ECG, respiration, motion, EMG, etc. Focusing on the heart activity only, a lot of methods are available for monitoring [1], such as electrocardiography (ECG) used as golden standard, ballistocardiography, phonocardiography, plethysmography, etc. However, such principles involve placement of electrodes and other sensors on the patient's body and require specific skills and knowledge. Additional problem is the amount of different sensors, which are also fragile and due to many reasons (placement, wires) can be obtrusive. A question arises whether some of these sensors can be replaced by only one universal and completely unobtrusive sensor.

The answer lies in the different types of sensors that can detect electrical, acoustic, or mechanical activity of the heart, even when there is no direct contact of the sensor with a person's body. Such advanced sensors receive signals generated by heart through the transmitting medium that is in a direct contact with the person, e.g. the bed or clothes. Heart activity is detected indirectly, conveyed thorough the medium, and in an entirely unobtrusive way. This field of research is lately quite popular and many approaches to unobtrusive heartbeat monitoring have been developed (a short survey is given in [2]).

An example of a flexible and very sensitive sensor for measuring mechanical, acoustic, and temperature impacts at the same time, is optical fibre. Feasibility of measuring heart rate by using fibre-optic interferometer has already been examined in [2] and [3]. Optical fibres were installed into a mattress, so that mechanical forces produced by heartbeats perturbed the fibres, what affected the interferometric signal. First method for detecting heartbeats from the interferometric signals was proposed on the signal zero-crossings and filter banks tuned to possible heartbeat frequencies [2]. The second approach applied was based on time-frequency representation by using pseudo Wigner-Ville distribution [3].

The fact is that different heart-activity features, respiration and, in part, also movement spread through disjoint frequency bands. It is well known that wavelet transform allows for multiresolutional analysis by applying a scheme of scaled wavelets whose frequency-domain characteristics correspond to band-pass filters. Hence, the output of wavelet transform yields time-scale representation that separates the features that do not overlap in the frequency or time domain. In order to estimate respiratory and heartbeat rates, two special filters with different bandwidths and central frequencies were constructed by using a linear combination of Morlet mother wavelets [4, 5]. Following the same goal, an analysis of fibre-optic interferometric signals was performed in [6].

In this paper, we study the discrimination ability of time-scale representation for different effects arising from the heart activity. It is based on fibre-optic signal transformed with Hilbert transformation and analysed by using Morlet wavelets in three different scales. The efficiency is evaluated for three heartbeat features: ballistocardiographic one and the first and the second heart sounds (S1 and S2).

II. METHODOLOGY

Optical sensor and signal

Our heartbeat detection method relies on a fibre-optic Michelson interferometer [7, 8]. It consists of laser diode (in our case telecom distributed feedback laser diode – DFB), sensing fibre, reference fibre, optical coupler, optical detector, and electronic converter (Fig. 1). Reference fibre is shielded mechanically by placing it in a loss tube, while the sensor fibre is put in a good contact either with the observed person's body directly or a transferring medium and the body indirectly. The optical coupler connects the laser diode and optical detector on one side with sensing and reference fibres on the other side. Unconnected fibre ends are covered by thin silver layer to enhance back reflection of the light waves. The coupler then functions as a splitter and combiner of back reflected light waves. Back reflected waves are added-up in the coupler (e.g. interfered). Minute changes in sensing fibre length thus cause significant changes in the phases of reflected light. This further means changes of the optical power that is detected by optical detector. The device has a cosine transfer characteristic. One period corresponds to a fibre length change that is equivalent to the half wavelength of the used optical source, which is 0.65 μm in our particular case (we used 1300 nm telecom DFB diode). Detected optical power is sampled at 2 kHz as interferometric signal $i(n)$, Eq. (1).

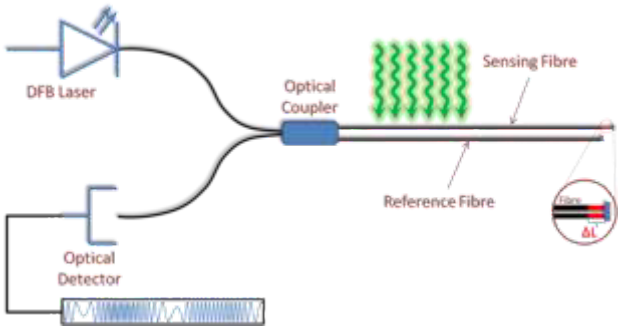

Fig. 1: Fibre-optic interferometer

The relationship between the external stimuli that stretch and shrink optical fibre and interferometric signal $i(n)$ is highly nonlinear. In order to derive the signal that represents such shortening and stretching of optical fibre, from the interferometric signal, it must be transformed by phase demodulation. Signal $i(n)$ is modelled as follows:

$$i(n) = A(n)\cos\left[s(n)\right] \tag{1}$$

where $A(n)$ stands for the interferometric signal amplitudes and $s(n)$ for a compositum of all the stimuli influencing the optical fibre. Analytic representation of such a signal can be derived by using the Hilbert transform:

$$\begin{aligned} y(n) &= x(n) + j \cdot H\left[x(n)\right] = \\ &= A(n)\left[\cos\left[s(n)\right] + j \cdot \sin\left[s(n)\right]\right] \end{aligned} \tag{2}$$

with j meaning the imaginary unit. Phase angle can be expressed as

$$\tan\phi(n) = \frac{\sin\left[s(n)\right]}{\cos\left[s(n)\right]} = \tan\left[s(n)\right] \tag{3}$$

By combining Eqs. (2) and (3), the phase of the analytic signal, $y(n)$, is computed:

$$\phi(n) = \tan^{-1}\left[y(n)\right] \tag{4}$$

The phase in Eq. (4) is wrapped due to the operation of arctangent function, $\tan^{-1}$. This means that a step with unwrapping must follow:

$$s(n) = unwrap\left[\phi(n)\right] \tag{5}$$

Consider now the derived external fibre-optic influences, $s(n)$, can be seen as a superimposition:

$$s(n) = s_{BR}(n)s_{HB}(n) + s_{MV}(n) + r(n) \tag{6}$$

where $s_{HB}(n)$ stands for the contribution of heartbeats, $s_{BR}(n)$ for the contribution of breathing, $s_{MV}(n)$ for the contribution of movement, and $r(n)$ for a residue whose main contents come from the ambiguity of unwrapped interferometric signal phase. It is caused by disability of locating the events when optical fibre reverts from stretching to shrinking and vice versa. Therefore, such reversals are inherently neglected during unwrapping, which means that $s(n)$ behaves as the optical fibre were only stretched all the time. For the same reason, the amplitudes of contributions of vital signs, $s_{HB}(n)$, $s_{BR}(n)$, and $s_{MV}(n)$, increase steadily, instead of increasing in the initial and decreasing in the termination phase of the event. Nevertheless, the contributions of different vital signs still remain unique and can be discerned.

Residue $r(n)$ includes also a superimposition of all disturbances, i.e. temperature noise, high-frequency random noise, and other environment influences (sounds and uncontrolled vibrations). It should be emphasised that the respiration modulates the amplitudes of heartbeat contributions in model (6).

Multiresolutional separation of interferometric signal components

Fibre-optic interferometric measurement acquires a compound signal whose components occupy partially non-overlapped frequency bands. This alludes one of possible discrimination approaches can be based on multiresolutional scheme of the wavelet transform.

The signal $s(n)$ can be transformed to time-scale representation W by using slightly modified version of continuous wavelet transform:

$$W(a,b) = \frac{1}{\sqrt{a}}\sum_{-\infty}^{\infty}\left(s(n) - \hat{s}_{a,b}(n)\right)\psi\left(\frac{n-b}{a}\right) \tag{5}$$

where a stands for scale, b for time lag, $\psi(n)$ for mother wavelet, and $\hat{s}_{a,b}(n)$ represents a local trend line in signal $s(n)$. The latter removes a linear trend from $s(n)$, according

to current scale a and time lag b. The signal segment covered by mother wavelet at scale a and time lag b is detrended prior to continuous wavelet transform, so that the signal sample values are decreased linearly between the wavelet onset and termination. This step is necessary due to monotonically increasing signal $s(n)$, as we explained in the previous subsection.

Morlet mother wavelet is used in our approach due to its compact time and frequency localization:

$$\psi(x) = e^{-\frac{x^2}{2}} \cos(5x) \tag{8}$$

III. EXPERIMENT AND RESULTS

Experimental protocol

Experimental protocol was designed to detect the mechanical and audible effects of cardiac activity by fibre-optic interferometer. Nine males and one female of age 31.30±10.45 years, height 177.50±7.04 cm, and weight 79.00±14.55 kg participated in the experiment. They were connected to a standard Schiller ECG device in order to acquire referential ECG signal in parallel with interferometric signals. We applied 4 electrodes on the extremities and lead II was taken as the referential one. Both the referential and interferometric signals were acquired by our own four-channel sampling device at 2000 Hz sampling rate. Hardware signal synchronization was applied.

After ECG referential electrodes mounted, participants were asked to reach their submaximal heart rate by cycling an ergometer [9]. Then, they immediately lied back down on the mattress and the interferometric and referential signal acquisition began simultaneously. Optical fibre was spirally bent on the stretchable (flexible) bed mattress and overlaid by a thin layer of foam. Subjects had to lie still and breathe normally through their nostrils. Interferometric and referential signals were acquired for 5 minutes. During this time, heart and respiration rate both decreased significantly. This kind of experimental protocol allowed for the dynamic changes of cardiac activity and, consequently, different mechanical and acoustic influences on optical fibre.

Multiscale analysis

Cardiac activity produces mechanical effects that may be evaluated by well-known ballistocardiographic approaches, also called mechanocardiography. Another established clinical examination, the so called phonocardiography, focuses of four different heart sounds as a consequence of audible cardiac activity.

We applied wavelet transform to fibre-optic interferometic signals and searched for the frequency components that belong to either ballisto- or phonocardiographic events of cardiac activity. The corresponding multiresolutional scheme depends on the scales involved in the computation of wavelets. Wavelets exhibit pass-band frequency characteristics. A simple relationship links scales, the wavelet's central frequency, and the desired frequency that fits the wavelet best:

$$a_i = \frac{f_c}{T \cdot f_i} \tag{7}$$

where f_c stands for the wavelet central frequency, T for sampling period, and f_i for the desired frequency.

Ballistocardiographic frequencies depend on heart rates. Our experimental protocol considers submaximal heart rates, which can be expected up to 180 bpm, i.e. 3 Hz. Therefore we decided to look for ballistocardiographic contents around 2.5 Hz. Phonocardiographic frequencies are not defined uniquely in the literature. Most definitions say the first heart sound (S1) extends from 10 to 140 Hz and the second one (S2) from 10 to 400 Hz [10]. Our intention was to verify whether heart sounds can be detected within fibre-optic interferometric signal or not. To be able to discern the contributions of the first and the second sound, we centered the two wavelet bands around 44 Hz (for S1) and 318 Hz (for S2). Using Morlet wavelets, the following scales correspond to the selected frequency bands: 780 for ballistocardiographic contributions, 44 for the first heart sound, and 6 for the second one.

Evaluation of results

Extensive studies have proved that heart sounds appear within well-defined time intervals after most intensive electrical heart activity, i.e. the R wave [10]. As our main goal was to find out whether or not cardiac mechanical and acoustic activity can be detected by fibre-optic interferometry, we measured delays from R waves to the highest amplitudes (energy) within the signal components filtered out by the wavelet transform at scales 780 (mechanical frequencies), 44 (S1), and 6 (S2).

Therefore, the first step was to locate the R waves in referential ECG recordings. This task was completed by using Pan-Tompkins QRS detection algorithm [11]. All false detected or undetected R waves were corrected manually. After that, the acquired fibre-optic interferometric signals were preprocessed with phase unwrapping and the obtained compound signals were analysed by the wavelet transform (Section II) in the three selected scales. An example of the outcomes on a short segment of the interferometric signal is collected in Fig. 2. Ballistographic component is depicted in the top row, heart sound S1 in the middle, and heart sound S2 in the bottom row of the figure. All three components were detected in the same segment of the interferometric signals, and so was the referential ECG which is depicted in red. Heart sounds were further processed by the Hilbert transform, which encapsulated the signal components into their envelopes. These served the signal energy maxima locating and every maximum was aligned with its nearest preceding R wave as found in the referential ECG. Distances from the R waves to the energy maxima were measured for each of the detected cardiac signal components.

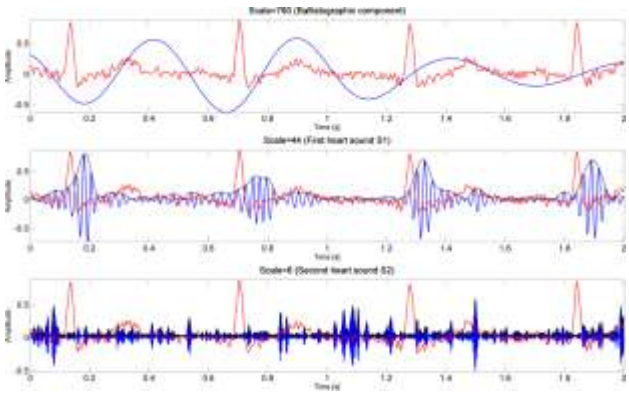

Fig. 2: An example of wavelet transform on a segment of interferometric signal $i(n)$; different frequency bands were filtered out for: ballistocardiographic components (top), heart sound S1 (middle), and heart sound S2 (bottom). Cardiac components are depicted in blue and encapsulated in black envelopes, while the referential ECGs appear in red.

Our first observation was about the second heart sound. The locations of detected energy maxima grouped into two classes. The first one concentrated up to 280 ms after R waves, the second one after this point in time. We denoted the two classes of the second heart sound by two indices as the earlier and later ones, $S2_e$ and $S2_l$, respectively. Time delays between estimated energy maxima and the corresponding R waves were statistically evaluated by means and standard deviations, yielding 226.50±104.60 ms, 48.91±21.48 ms, 124.68±76.30 ms, and 418.69±89.82 ms for ballistocardiographic, S1, $S2_e$, and $S2_l$ components, respectively. Detailed results for all tested subjects are collected in Fig. 3 for ballistocardiographic components, Fig. 4 for sounds S1, Fig. 5 for sounds $S2_e$, and Fig. 6 for sounds $S2_l$.

Distances between successive detections in the individual signal components, i.e. ballistocardiographic and heart sounds, were also compared to referential RR intervals. Mean and median relative errors were computed. For each of the calculated errors, dispersion was assessed by using 90th percentile P_{90}, yielding the value with 90% of errors below it. The results are depicted in Figs.7, 8, 9, and 10.

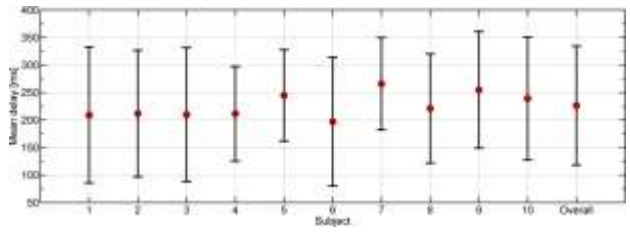

Fig. 3: Delays between R waves and the energy maxima in ballistocardiographic components as detected in scale 780 by the wavelet transform of interferometric signals: means denoted by red spots, standard deviations by upright lines.

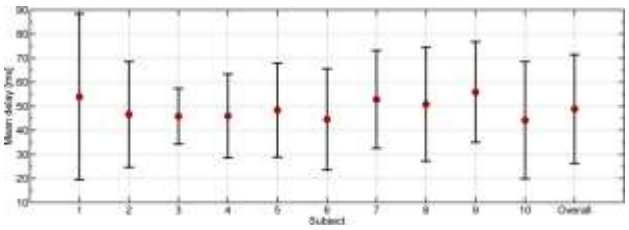

Fig. 4: Delays between R waves and the energy maxima in the first heart sound, S1, as detected in scale 44 by the wavelet transform of interferometric signals: means denoted by red spots, standard deviations by upright lines.

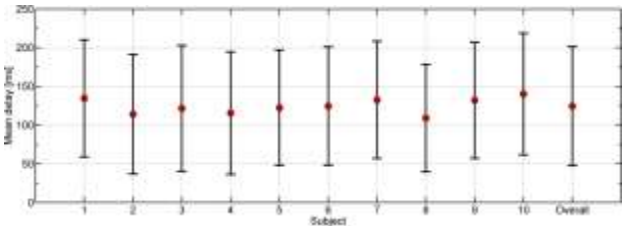

Fig. 5: Delays between R waves and the energy maxima in the second heart sound $S2_e$ as detected in scale 6, earlier than 280 ms after R, by the wavelet transform of interferometric signals: means denoted by red spots, standard deviations by upright lines.

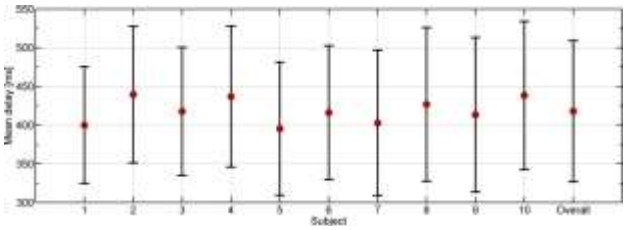

Fig. 6: Delays between R waves and the energy maxima in the second heart sound $S2_l$ as detected in scale 6, later than 280 ms after R, by the wavelet transform of interferometric signals: means denoted by red spots, standard deviations by upright lines.

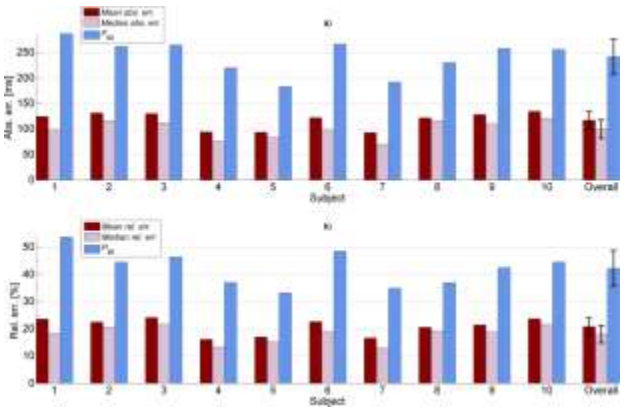

Fig. 7: Mean errors, median errors, and dispersion of mean errors determined by P_{90} are measured between the intervals of detected maxima in the ballistocardiographic components and corresponding referential RR intervals: a) absolute errors; b) relative errors.

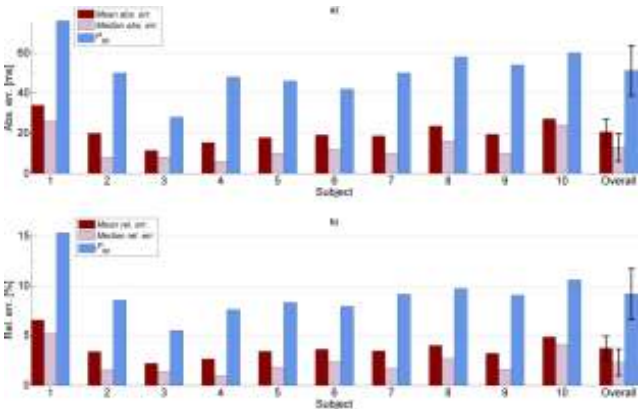

Fig. 8: Mean errors, median errors, and dispersion of mean errors determined by P_{90} are measured between the intervals of detected maxima in the first heart sounds and corresponding referential RR intervals: a) absolute errors; b) relative errors.

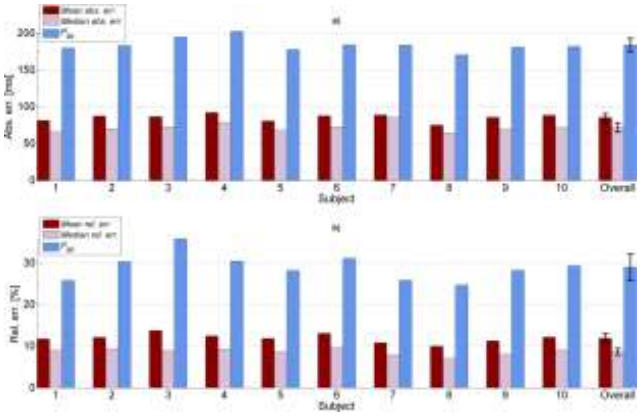

Fig. 9: Mean errors, median errors, and dispersion of mean errors determined by P_{90} are measured between the intervals of detected maxima in the second heart sounds, when appearing earlier than 280 ms after R, and corresponding referential RR intervals: a) absolute errors; b) relative errors.

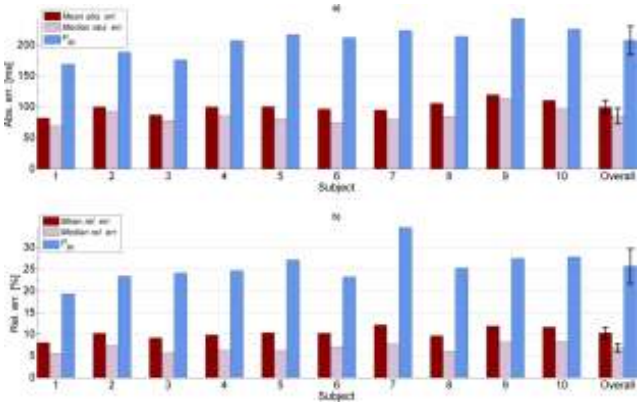

Fig. 10: Mean errors, median errors, and dispersion of mean errors determined by P_{90} are measured between the intervals of detected maxima in the second heart sounds, when appearing later than 280 ms after R, and corresponding referential RR intervals: a) absolute errors; b) relative errors.

IV. DISCUSSION AND CONCLUSIONS

Our experiments prove that fibre-optic interferometry is sensitive enough to react to even weak mechanical or acoustic perturbations caused by human vital signs. Moreover, we were able to detect and discern the different signal components that accompany cardiac activity. Due to non-overlapping frequency contents of ballistocardiographic and phonocardiographic contributions, these components were successfully separated by applying a multiresolutional scheme based on Morlet wavelets.

The following frequency bands are recommended for observing cardiac responses: 0.1-20 Hz, 10-140 Hz, and 10-400 Hz for the ballistocardiographic component and the first and the second heart sound [10]. We focused on the frequencies where, at least to our experience, the vast majority of energy may be expected: up to 2.5 Hz for ballistocardiographic, and around 44 Hz and 318 Hz for phonocardiographic components. The corresponding scales were calculated by Eq. (7) and set to 780, 44, and 6 for the three components.

Our most important goal was to verify whether or not the applied multiresolutional signal decomposition is representative, meaning that the obtained signal components show the properties that actually characterize ballisto- and phonocardiographic recordings. As we limited our detection to preselected frequency bands that certainly contain the observed phenomena, the detections had to be confirmed by different evidence. We decided to estimate the delays of the detected energy maxima after the referential R waves (Figs. 3, 4, 5, and 6). Previous studies claim the first heart sound, S1, must appear 10-50 ms after the R wave and its duration is about 100-160 ms, whereas the second heart sound, S2, appears 280-360 ms after the R wave and its duration can be 80-140 ms [10]. For the ballistocardiography, most of low-frequency energy is concentrated in-between the two heart sounds, S1 and S2, so that it must be located approximately between 150 and 400 ms after the R wave [12].

The overall estimations according to our experiments yield the following average locations: 226.50±104.60 ms, 48.91±21.48 ms, 124.68±76.30 ms, and 418.69±89.82 ms after referential R waves for ballistocardiographic and phonocardiographic components, S1, $S2_e$, $S2_l$, respectively. These figures coincide well with physiological expectations, except for the second sound $S2_e$ in its earlier detection. However, it is known that the second heart sound can split because of an unsynchronised closure of aortic and pulmonary valves, producing two segments 20-80 ms apart. This may explain why we detected maxima of S2 located at 124.68±76.30 ms for 61.01±6.40% of all the detected heartbeats, and located at 418.69±89.82 ms after the R waves for the rest of beats. Additional experiments and evaluation would be necessary to confirm this speculation.

We also compared the inter-beat distances, as detected by either ballisto- or phonocardiographic energy maxima, to the referential RR intervals. Figs. 7, 8, 9, and 10 show the mean relative errors are 20.83±3.12%, 3.74±1.22%, 11.96±1.07%, and 10.33±1.27% for ballistocardiographic

components and heart sounds S1, $S2_e$, and $S2_l$, respectively. Two conclusions can be drawn upon this statistics. Firstly, the regularity and stability of the detected signal components when compared to referential RR intervals reinforce the belief that the detections can be considered reliable and, therefore, represent the actual physiological phenomena. And secondly, the first heart sound location is the most stable, while the ballistocardiographic readings vary the most. Both second heart sound locations show a medium variance.

Finally, we believe the proposed multiresolutional analysis of fibre-optic interferometric signals can discern ballistocardiographic and phonocardiographic contributions of cardiac activity with high reliability. The most robust measure of heartbeats appears to be the first heart sound, whereas the ballistocardiographic detections do not prove that reliable and accurate.

V. ACKNOWLEDGEMENT

All persons signed an informed consent to participate in our experimental protocols that were approved by the National Medical Ethics Committee of the Republic of Slovenia (no. 81/10/10). We also acknowledge partial financial support of the Slovenian Ministry of Education, Science, Culture, and Sport (contract no. 3211-10-000464 for the Competence Centre of Biomedical Engineering).

REFERENCES

1. Ranganathan N, Sivaciyan V, Saksena FB (2006) The Art and Science of Cardiac Physical Examination. Totowa, NJ: Humana Press.
2. Šprager S, Đonlagić D, Zazula D. Monitoring of Basic Human Vital Functions Using Optical Interferometer. IEEE 10th International Conference on Signal Processing ICSP 2010, Beijing, China, 2: 1738-1741.
3. Šprager S, Đonlagić D, Zazula D. Heart Beat Monitoring Using Optical Interferometric Signal and Pseudo Wigner-Ville Distribution. The 7th International Conference on Information Technology and Applications ICITA 2011, Sydney, Australia, 271-275.
4. Chan Y (1995) Wavelet basics. Springer.
5. Mallat S (1999) A wavelet tour of signal processing. Academic Press.
6. Šprager S, Đonlagić D, Zazula D. Estimation of Heart Rate, Respiratory Rate and Motion by using Optical Interferometer as Body Sensor. Proceedings of the IASTED International Conference on Signal and Image Processing 2011, Dallas, USA, 280-287.
7. Udd E (1991) Fiber Optic Sensors - An Introduction for Engineers and Scientists, John Wiley & Sons.
8. Šprager S, Cigale B, Đonlagić D, Zazula D. A wavelet-based detection of active segments in optical interferometer caused by fibre strain. Proceedings of the 10th WSEAS international conference on communications, electrical & computer engineering, and 9th WSEAS international conference on Applied electromagnetics, wireless and optical communications, Gran Canaria, Spain, 2011, 123-127.
9. Tanaka H, Monahan KD, Seals RD. Age-predicted maximal heart rate revisited. Journal of the American College of Cardiology, 2001, 37:153-156.
10. Ahlström C. Nonlinear Phonocardiographic Signal Processing. Dissertation. Linköping University, Sweden, 2008.
11. Pan J, Tompkins WJ. A real-time QRS detection algorithm. IEEE Transactions on Biomedical Engineering, 1985, 3:230-236.
12. Pinheiro E, Postolache O, Girao P. Theory and Developments in an Unobtrusive Cardiovascular System Representation: Ballistocardiography. The Open Biomedical Engineering Journal, 2012, 4:201-216.